Polymer Vol. 39 No. 22, pp. 5335–5341, 1998

0032-3861/98/$ - see front matter

PII: S0032-3861(97)10233-6

Application of a continuous zone-drawing method to nylon 66 fibres

Akihiro Suzuki*, Yu Chen and Toshio Kunugi
Department of Applied Chemistry and Biotechnology, Faculty of Engineering, Yamanashi University, 4-3-11 Takeda, Kofu 400–8511, Japan
(Received 21 August 1997; revised 13 October 1997; accepted 21 October 1997)

A continuous zone-drawing (CZD) treatment was applied to nylon 66 fibres in order to improve their mechanical properties. The CZD treatment was carried out at a drawing rate of 420 mm/min and in three steps; the first CZD (CZD-1) at a drawing temperature of 210°C under an applied tension of 30.3 MPa, the second (CZD-2) at 220°C under 229.5 MPa, and the third (CZD-3) at 230°C under 364.9 MPa. The orientation factor of crystallites reached a high value of 0.960 with only the CZD-1 treatment, but that of an amorphous phase increased with the number of times in CZD treatment. The *trans* isomer content increased during the CZD treatment, whereas the *gauche* decreased. The CZD-3 fibre had a value of birefringence of 0.072, a degree of crystallinity of 37%, a tensile modulus of 8 GPa, and a tensile strength of 1.2 GPa. © 1998 Elsevier Science Ltd. All rights reserved.

(Keywords: continuous zone-drawing; nylon 66; tensile modulus)

INTRODUCTION

To impart superior mechanical properties to nylon fibres, many techniques have so far been proposed[1–4]. We have also proposed a zone-drawing and zone-annealing[5], a high-temperature zone-drawing[6,7], and a high-tension annealing[8] method. These methods are some of the techniques leading to high-performance nylon fibres. However, the length of treatable fibre at any one time is limited because these methods are under batchwise operations. These methods may command considerable interest from a scientific point of view, but are perhaps of lesser interest to industrial scientists.

To continuously draw and/or anneal fibres at higher treating speeds, an apparatus was specially designed and assembled in our laboratory. The drawing and annealing treatment using the apparatus, that is, a continuous zone-drawing and zone-annealing method has already been applied to poly(ethylene terephthalate) fibre[9]. We reported that the treatment had the same effect on improving the mechanical properties as in the case of the batchwise zone-drawing and zone-annealing treatment that was previously reported[10].

The objective of the present study is to improve the mechanical properties of nylon 66 fibres by applying the continuous zone-drawing method. The changes in the microstructure and mechanical properties of the continuously drawn nylon 66 fibres were investigated by tensile testing, dynamic viscoelasticity, differential scanning calorimetry (d.s.c.), thermal mechanical analysis (TMA), X-ray diffraction, density, and birefringence measurements.

EXPERIMENTAL

Material

The original material used in the present study is the as-spun single nylon 66 fiber supplied by TORAY Ltd. The original fibre had a diameter of 0.519 mm, a degree of crystallinity of 25%, and a value of birefringence of 1.1×10^{-3}.

Apparatus for continuous zone-drawing

A schematic diagram of the apparatus used for the CZD treatment is given in *Figure 1*. The apparatus consists of supplying and windup spools, a temperature-controlled zone-heater, a movable pulley, a traverse, speed control motors, and a laser displacement sensor system. The fibre is unwound from the supplying spool and passes through a temperature-controlled zone-heater, through a movable pulley between two guide pulleys and finally is wound on the winding spool after passing through a traverse. The supplying and windup spools were attached to the shafts of speed control motors. The speed of the supplying motor was arbitrarily adjusted in the speed range of 12 to 186 rpm by a potentiometer, and that of the windup motor was automatically controlled by a laser displacement sensor system, as described below. To check the speed of each motor, digital speed indicators were connected to the two motors. A tension on the fibre was arbitrarily applied by hanging a weight on the hook attached to the movable pulley. The positioning control of the movable pulley was carried out by the laser displacement sensor system. This system consists of a laser sensor head, a controller, and an analogue sensor controller. The analogue sensor controller was attached to supply an analogue voltage which corresponds to the change in the position of the movable pulley to the windup motor. Thus, the speed of the windup motor was automatically regulated by the system so that the movable pulley could be operated in a constant position.

Measurement

Draw ratio was determined in the usual way by measuring the displacement of ink marks placed 10 mm apart on the fibre prior to drawing. Birefringence was measured with a

* To whom correspondence should be addressed

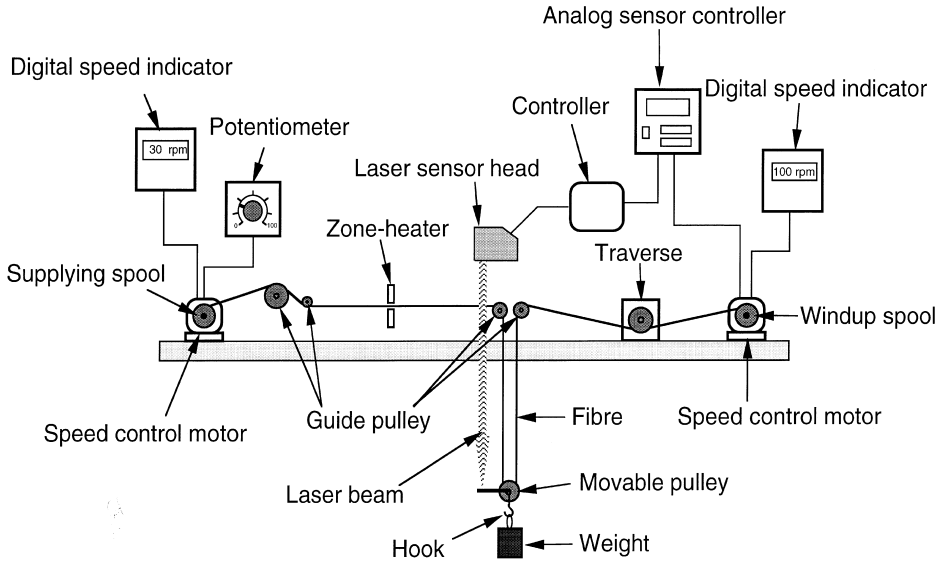

Figure 1 Scheme of apparatus used for continuous zone-drawing (CZD)

polarizing microscope equipped with a Berek compensator. The density (d) of each fibre was measured by flotation technique using a carbon tetrachloride and toluene mixture. An apparent mass crystallinity (X_w) was obtained using the relation:

$$X_w = \frac{d_c(d - d_a)}{d(d_c - d_a)} \times 100 \quad (1)$$

where d_c and d_a are densities of crystalline and amorphous phases, respectively. In this measurement, a value of 1.24 g/cm^3 was assumed for d_c, and a value of 1.09 g/cm^3 for d_a[11].

Orientation factors of crystallites (f_c) were evaluated by using the Wilchinsky method[12] from wide angle X-ray diffraction patterns. Amorphous orientation factors (f_a) were calculated by:

$$f_a = \frac{\Delta n - \Delta n_c^\circ f_c X_v}{\Delta n_a^\circ (1 - X_v)} \quad (2)$$

where X_v is the crystallinity in volume fraction, Δn_c° an intrinsic crystallite birefringence, and Δn_a° an intrinsic amorphous birefringence. The intrinsic birefringences were taken to be 0.096 and 0.077[13]. Apparent crystallite sizes were estimated from the broadening of the diffraction peaks by applying Scherrer's equation:

$$D_{hkl} = \frac{0.9\lambda}{\beta \cos \theta_{hkl}} \quad (3)$$

where D_{hkl} is the crystallite width normal to (hkl) plane, λ is the X-ray wavelength (1.542 Å), θ_{hkl} is the Bragg angle of the (hkl) plane, and β is the observed half-width of the peak, which was corrected for the instrumental broadening.

Fourier-transform infrared (*FT*i.r.) spectra of nylon 66 fibres were obtained at room temperature on a Perkin Elmer *i*-Series *FT*i.r. microscope connected to a Perkin Elmer Paragon 1000 spectrometer. The spectra were measured at 4 cm^{-1} resolution and 312 scans.

The d.s.c. measurements were carried out using a Rigaku d.s.c. 8230 C calorimeter. The d.s.c. scans were performed over the temperature range from 25 to 280°C, using a heating rate of 10°C/min in a nitrogen gas atmosphere.

Thermal shrinkage was measured with a Rigaku SS-TMA and was measured over the temperature range from 25 to 230°C at a heating rate of 5°C/min. The samples with a 15 mm gauge length between two jaws were held under a tension of 5 g/cm^2, which was the minimum tension to stretch a fibre tightly.

Tensile properties were determined on a Tensilon tensile testing machine (Orientec Co. Ltd.). Tensile modulus, tensile strength and elongation at break were determined from the stress–strain curves that were obtained at 25°C and 65% relative humidity. Dynamic viscoelastic properties were measured at 110 Hz with a dynamic viscoelastometer vibron DDV-II (Orientec Co. Ltd.). Measurement was carried out over a range of temperature from about 25 to 230°C at temperature intervals of 5°C. The average heating rate was 2°C/min.

RESULTS AND DISCUSSION

Conditions for the CZD treatments

The CZD treatment was carried out in three steps. The optimum condition for each step was decided from the values of birefringence (Δn) of the fibres obtained under various conditions; the condition giving the highest Δn was chosen as the optimum one for each step. Preliminary experiments determined that 420 mm/min was the optimum supplying speed and this was used throughout the CZD treatments. *Figure 2* shows the changes in the draw ratio (λ) and Δn of each CZD-1 fibre drawn under three different applied tensions (σ_a) with a drawing temperature (T_d). The λ values of the fibres drawn under three different σ_a values increase with increased T_d, but the Δn values of two fibres, except for that of the fibre drawn under the lowest σ_a = 20.9 MPa, increase at first and decrease with T_d. The Δn values of two fibres drawn under σ_a = 25.6 and 30.3 MPa show the maximum values at T_d = 210°C; the fibre drawn under σ_a = 30.3 MPa gives the highest Δn of 0.062. The decrease in Δn shows that the fluid-like deformation caused the slippage among amorphous chains that occurred during the drawing process at T_d = 220°C. Consequently, the condition giving the highest Δn was chosen as the optimum one for the CZD-1 treatment.

The optimum conditions for the second (CZD-2) and the third (CZD-3) treatments were also determined in the same

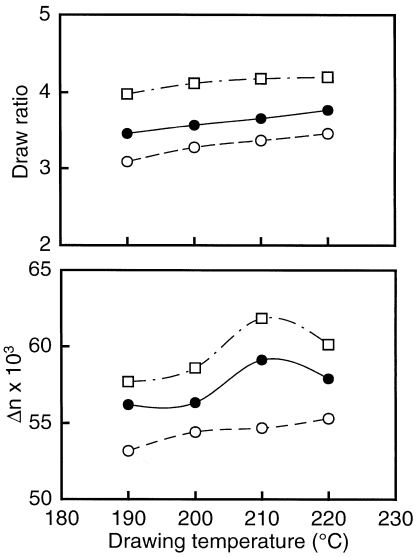

Figure 2 Changes in the draw ratio (λ) and birefringence (Δ*n*) of the CZD-1 fibres drawn under three different applied tensions (σ_a) with a drawing temperature (T_d): ○, $\sigma_a = 20.9$ MPa; ●, $\sigma_a = 25.6$ MPa; □, $\sigma_a = 30.3$ MPa

Table 1 Optimum conditions for the continuous zone-drawing and high temperature zoned-drawing treatments

Step	Drawing temperature (°C)	Applied tension (MPa)	Drawing speed (mm/min)
CZD-1	210	30.3	
CZD-2	220	229.5	420
CZD-3	230	364.9	
HT-ZD1	210	29.4	
HT-ZD2	220	284.1	50
HT-ZR3	230	411.6	

way as in the case of the CZD-1 treatment. Furthermore, though we attempted the fourth CZD (CZD-4) treatment, the Δ*n* could not be improved further by the CZD-4 treatment. The optimum conditions for the CZD-1, the CZD-2, and the CZD-3 treatments, together with those for the high-temperature zone-drawing (HT-ZD) treatments reported previously[6], are summarized in *Table 1*. The optimum conditions of the CZD treatments were approximately the same, except for the drawing rate, as those of the HT-ZD treatments. The drawing rate in the CZD treatments is 8.4 times faster than that in the HT-ZD treatments.

Microstructure for the CZD fibres

Figure 3 shows the relation between λ and Δ*n*. The latter increases linearly with λ and up to 0.072 for the CZD-3 fibre. Ward *et al.*[14] reported that Δ*n* increased linearly with increasing λ at a lower level, but levelled off to reach a saturated value at higher values of λ. This indicates that the intermolecular linkage is broken down, and as a result the polymer molecules may slip past one another and flow individually. In our experiment, however, such saturation in the Δ*n* values was not observed, and the molecular draw ratio corresponds well with the macroscopic draw ratio. This proved that the chain slippage leading to disorientation did not occur during the CZD treatments.

Table 2 lists the degree of crystallinity (X_w), orientation factors of crystallites and amorphous regions (f_c and f_a), and apparent crystallite sizes normal to the (100) reflection and

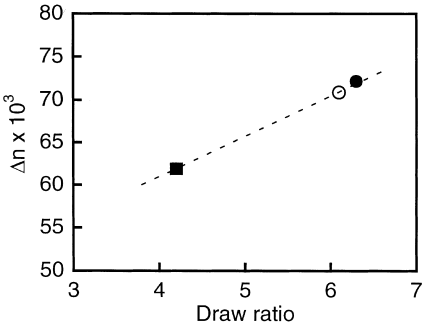

Figure 3 Relation between draw ratio (λ) and birefringence (Δ*n*): ■, CZD-1 fibre; ○, CZD-2 fibre; ●, CZD-3 fibre

the (010)/(110) doublet (D_{100}, and $D_{010/110}$) for the CZD fibres. The D_{100} represents the interchain distance within the hydrogen-bonded sheets, and the unresolved doublet $D_{010/110}$ is related to intersheet distance. X_w increases stepwise with the number of times in CZD treatment, and the CZD-3 fibre has a degree of crystallinity of 37%. The value of X_w is 13% lower than the limiting crystallinity of 50% in nylon 66. The increment in X_w suggests there is an increase in the number of crystallites and/or a crystal growth during the treatments. D_{100} and $D_{010/110}$ increase slightly with the number of times in CZD treatment. It is presumed that the crystal growth proceeded perpendicular to the fibre axis by additional crystallization. However, the highly oriented crystallites probably grow along the fibre axis by further crystallization. Penszkin *et al.*[15] studied the kinetics of crystallization of annealed PET fibres by wide-angle X-ray diffraction and small-angle X-ray scattering measurements. They reported that the growth of oriented crystals along the fibre axis occurred at constant thickness perpendicular to the fibre one. f_c increases up to 0.960 near to unity with only the CZD-1 treatment and further to 0.987 with subsequent treatments. The crystallites are easily aligned in the drawing direction in the same manner as in the cases of various kinds of fibres reported[5–9] previously. Murthy *et al.*[16] studied the changes in orientation of the crystalline and amorphous regions of nylon 6 fibres during drawing and annealing. They showed that the crystalline orientation increased rapidly at small draw ratios (< 3) and reached a plateau at higher draw ratios. On the other hand, f_a increases from 0.641 for the CZD-1 fibre to 0.795 for the CZD-3 fibre with the number of times in CZD treatment. Unlike f_c, f_a is strongly dependent on the number of treatments. The amorphous orientation is closely related to the mechanical properties as described below.

Figure 4 shows the *FT*i.r. spectra limited to 700–1800 cm^{-1} for the original and CZD fibres. To monitor conformational changes during the CZD treatments, the bands situated at 936 and 1146 cm^{-1} were used[17]. The former is attributed to a *trans* conformation, and the latter to a *gauche* conformation. The *trans* conformation can be involved in the crystalline and the amorphous phases, but the *gauche* conformation can be found only in the amorphous phase. In this study, the band at 1650 cm^{-1} was used as an internal reference band because it appears this band is not affected by the treatments. *Table 3* lists the intensities of the bands situated at 936, 1146 and 1650 cm^{-1} and the intensity ratios (I_{936}/I_{1650} and I_{1146}/I_{1650}). The I_{936}/I_{1650} value for the *trans* conformation increases with the number of times in CZD treatment, whereas the I_{1146}/I_{1650} value for the *gauche* one decreases due to the

Table 2 Crystallinity (X_w), crystallite orientation factor (f_c), amorphous orientation factor (f_a) and crystallite size (D_{hkl}) for the CZD fibers

Fibre	X_w (%)	f_c	f_a	D_{100} (Å)	$D_{010/110}$ (Å)
CZD-1	32	0.960	0.641	26.8	26.6
CZD-2	36	0.987	0.784	29.9	28.0
CZD-3	37	0.987	0.795	32.3	30.1

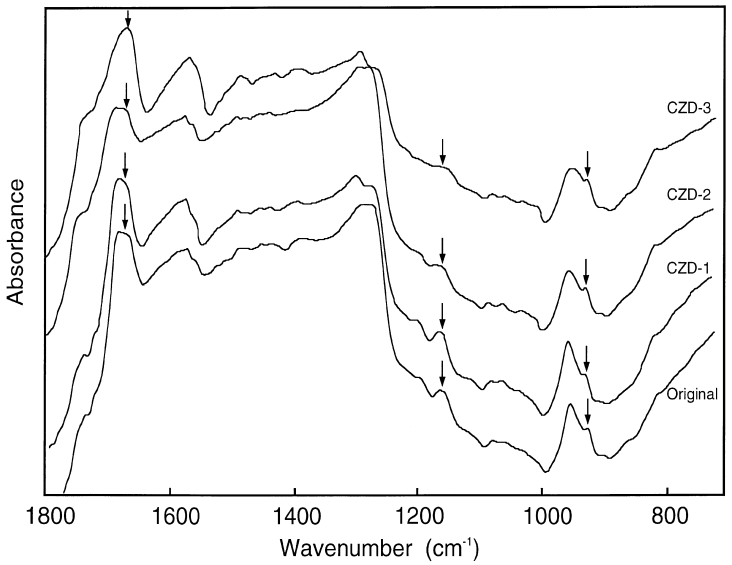

Figure 4 *FT*i.r. spectra of the original and CZD fibres in the spectral range 700–1800 cm^{-1}

Table 3 Absorbances of bands at 936, 1146, and 1650 cm^{-1} and relative absorbances for the original and CZD fibres

Fibre	I_{936}	I_{1146}	I_{1650}	$I_{936/1650}$	$I_{1146/1650}$
Original	0.160	0.073	0.431	0.378	0.169
CZD-1	0.251	0.067	0.476	0.527	0.165
CZD-2	0.193	0.044	0.335	0.576	0.131
CZD-3	0.179	0.029	0.309	0.579	0.094

conformational changes that occurred during the CZD treatments. Furthermore, to carry out the quantitative analysis, an isomer content was estimated using a two-phase conformational model. Quintanilla *et al.*[17] proved that nylon 66 as well as PET[18] satisfied this model:

$$I = p_1 \frac{I_{936}}{I_{1650}} + p_2 \frac{I_{1146}}{1_{1650}} \quad (4)$$

where p_1 and p_2 are 936 and 1146 cm^{-1} band weights, which are related to the interaction of radiation matter. Equation (4) is rewritten as follows:

$$\frac{I_{1650}}{I_{1146}} = p_1 \frac{I_{936}}{I_{1146}} + p_2 \quad (5)$$

This linear relation between the intensity ratios is required to verify the model for nylon 66; *Figure 5* shows a good fitting with the experimental values from the *FT*i.r. measurements. The least-squares curve fitting technique was carried out to obtain the p_1 and p_2 parameters. The values of the products $p_1(I_{1650}/I_{1146})$ and $p_2(I_{936}/I_{1146})$ represent the *trans* and *gauche* distributions. *Figure 6* shows the individual isomer content for the original and CZD fibres. The *trans* isomer content increases stepwise with the number of times in CZD treatment, whereas the *gauche* content decreases. It seems that the conformational changes result from the morphological change of a chain-folded crystalline structure into a fringed-micelle structure and an extension of amorphous chains.

Figure 7 shows a d.s.c. thermogram for each of the original and CZD fibres. The original fibre shows the broad melting peak at 258°C, and there is a trace of a shoulder on the low temperature side. The d.s.c. thermogram of the CZD-1 fibre has a double melting peak; a high-temperature melting peak locates at 258°C that is the same temperature as in the case of the original fibre, and low-temperature one at 254°C. The appearance of a low-temperature melting peak is attributable to the morphological transformation of crystallite; the chain-folded crystalline structure of original fibre changes partially into a fringed-micelle one with an unfolding of the chains. Elenga *et al.*[19] suggested from the standpoint of kinetics that the low-temperature melting peak was ascribed to the fringed-micelle crystals built up by chain unfolding and the high-temperature one corresponds to the untransformed fraction of the lamellar crystals which undergo reorganization during the heating scan. Furthermore, they indicated that the low temperature melting crystals were unlikely to recrystallize into more stable crystals during the d.s.c. scan. On the other hand, Fakirov *et al.*[20] proposed that the appearance of the double melting peak in annealed PET fibres was relevant to the melting and

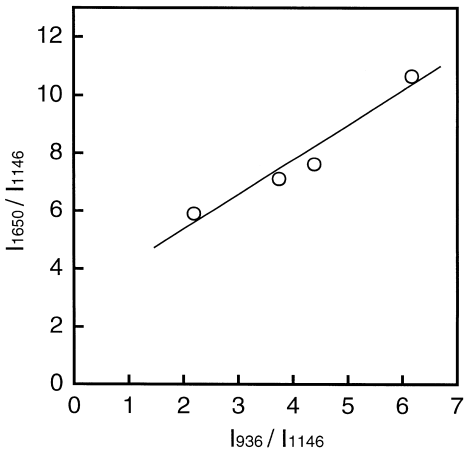

Figure 5 Relation between the I_{1650}/I_{1146} and I_{936}/I_{1146} in nylon 66

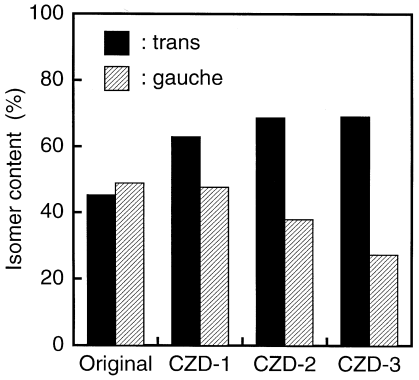

Figure 6 *Trans* and *gauche* isomer content for the original and CZD fibres

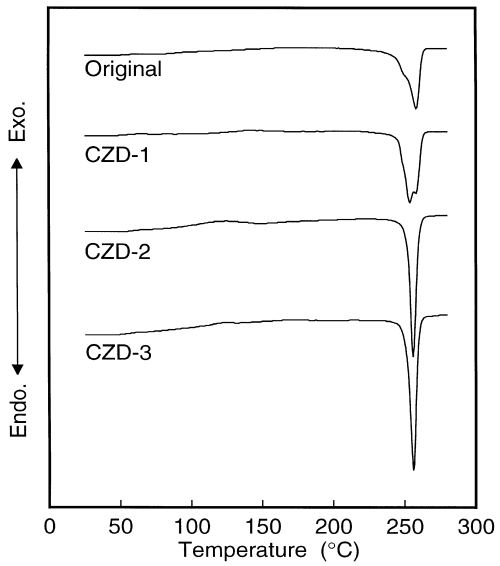

Figure 7 d.s.c. thermograms of the original and CZD fibres

partial recrystallization during the d.s.c. scan. The CZD-2 and CZD-3 fibres have only sharp peaks at 256°C, but the high-temperature melting peaks in their thermograms are absent. If the low-temperature melting crystals were recrystallized into more stable crystals during the d.s.c. scan, the CZD-2 and CZD-3 fibres would have the double melting peak in the same manner as in the case of the CZD-1 fibre, too. The appearance of a single melting peak supposes that the chain-folded crystals remained in the CZD-1 fibre change into the fringed-micelle crystals during the CZD-2 treatment, and that the recrystallization of the crystals induced by the CZD-1 treatment does not occur during the d.s.c. scan. The morphological change of the chain-folded crystals into the fringed-micelle crystals was supported by the spectral change in *FT*i.r. measurements as described above. The CZD treatments shift the melting peak to slightly higher temperatures and result in a sharpening of the melting peaks. This trend is consistent with an increase in crystal size and/or crystal perfection[21,22].

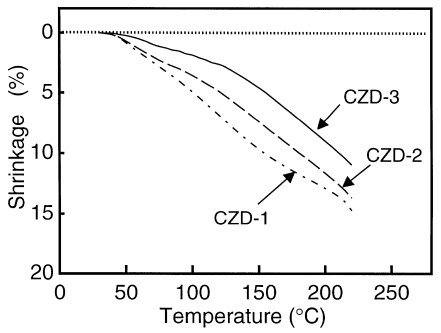

Figure 8 Temperature dependence of thermal shrinkage for the CZD fibres

Figure 8 shows the temperature dependence of the thermal shrinkage for the CZD fibres. The CZD fibres begin to shrink from 35°C with increasing temperature, and a degree of the shrinkage decreases with the number of times in CZD treatment. The CZD-3 fibre of $X_w = 37\%$ has the lowest degree of shrinkage in comparison with other fibres. The thermal shrinkage during heating is associated with the chain folding in the oriented amorphous regions[23] and occurs above a glass transition temperature (T_g). However, the shrinkage in the case of the CZD fibres occurs even in the temperature range below the T_g (=50°C). The shrinkage below T_g indicates that there occurred a small rubber-elastic contraction of tie molecules above the subglass transition temperature (β relaxation). In the β relaxation the non-hydrogen bonded amide groups begin to move, but this effect is not sufficient to overwhelm the expansion of their adjacent amorphous components[24]. The large-scale segmental motion in amorphous regions above the T_g is prevented by the crystallites acting as crosslinking points[25]. Furthermore, Choy *et al.*[24] reported that the presence of oriented chains and taut tie molecules in the amorphous regions is likely to inhibit the thermal shrinkage. The difference in the shrinkage behaviour among the CZD fibres is due to a crosslinking density of a physical network built up by the crystallites. In the case of the CZD-1 fibre having the lower degree of crystallinity, the physical network was insufficient for constraint of the thermal shrinkage compared with other fibres. The crosslinking density increases with increasing degree of crystallinity, and then the chain refolding becomes increasingly difficult. A slight increase in the slope of the thermal shrinkage curves is shown above 100°C. The slight increase is attributable to the decrease in the density of the entangled molecular network and to the rupture of hydrogen bonds inhibiting the chain refolding.

Mechanical properties for the CZD fibres

Table 4 lists the tensile properties of the CZD fibres. The CZD-3 fibre has a tensile modulus of 8 GPa and a tensile

Table 4 Tensile properties of the CZD fibres

Fibre	Tensile modulus (GPa)	Tensile strength (GPa)	Elongation at break (%)
CZD-1	5	0.7	28
CZD-2	7	1.1	12
CZD-3	8	1.2	11

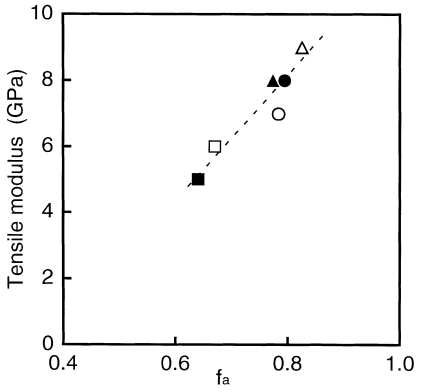

Figure 9 Relation between the tensile modulus and amorphous orientation factor (f_a): ■, CZD-1 fibre; ○, CZD-2 fibre; ●, CZD-3 fibre; □, HT-ZD1 fibre; ▲, HT-ZD2 fibre; △, HT-ZD3 fibre

strength of 1.2 GPa. Although there is a significant difference in the drawing speed between the CZD and the HT-ZD treatments, the tensile modulus and the tensile strength are nearly equal to those of the HT-ZD nylon 66 fibres that were previously reported (9 GPa and 1.4 GPa)[6]. Furthermore, the tensile modulus of the CZD-3 fibre is almost two times higher than that of the commercial fibres[26] (3.9 GPa). However, the tensile modulus obtained is lower than that (12.3 GPa) of high-tension annealed nylon 66 fibre[8]. The improvement in the tensile moduli of semi-crystalline polymers such as nylon and PET is usually achieved by increasing the orientation of the crystallites and the amorphous regions[27]. Because the f_c of the CZD-1 fibre reached a higher value near to unity as described above, the improvement in the modulus appears to be influenced by the f_a rather than the f_c. It can be seen from *Figure 9* that the tensile modulus increases linearly with increasing f_a. The linear relation was also found in the case of the HT-ZD nylon 66 fibres that were previously reported[6].

Figure 10 shows the temperature dependence of storage modulus (E') for the original and CZD fibres. The E' values over a wide temperature range increase progressively with the number of times in CZD treatment. Finally, the E' value of the CZD-3 fibre reaches 8.1 GPa at 25°C. The E' values of all the fibres decrease gradually with increasing temperature. *Figure 11* shows temperature dependence of tan δ for the original and CZD fibres. The CZD fibres show α peaks in the temperature range of 80 to 120°C, considered to originate from a rupture of interchain hydrogen bonding due to the motions of chain segments in amorphous regions[28]. The α peak shifts to a higher temperature and decreases in its peak height, and becomes much broader with the number of times in CZD treatment. The changes in position and in profile of the α peak with the number of times in CZD treatment designate that the molecular mobility in the amorphous regions is restricted by the physical network built up by the crystallites.

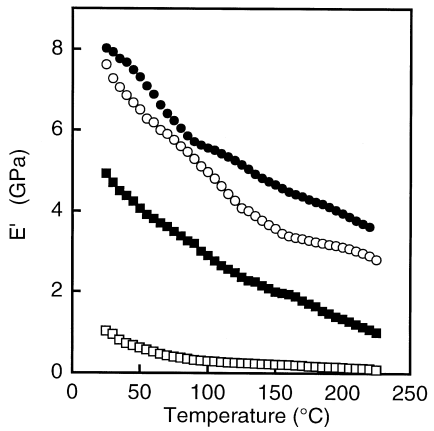

Figure 10 Temperature dependence of storage modulus (E') for the original and CZD fibres: □, original fibre; ■, CZD-1 fibre; ○, CZD-2 fibre; ●, CZD-3 fibre

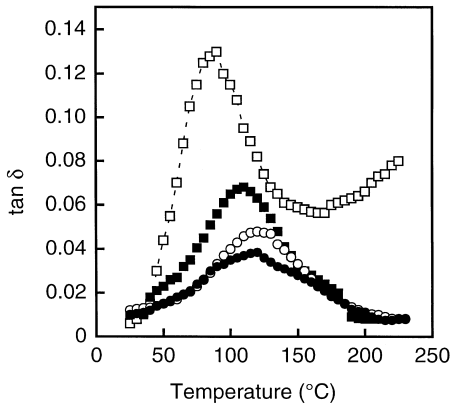

Figure 11 Temperature dependence of tan δ for the original and CZD fibres: □, original fibre; ■, CZD-1 fibre; ○, CZD-2 fibre; ●, CZD-3 fibre

CONCLUSION

The continuous zone-drawing (CZD) method has been applied to nylon 66 fibres to improve their mechanical properties, and the results are as follows.

(1) The degree of crystallinity increased from 25% for the original fibre to 37% for the CZD-3 fibre. The orientation factor of crystallites increased remarkably up to 0.960 with the CZD-1 treatment. On the other hand, the amorphous orientation factor increased with the number of times in CZD treatment.

(2) To quantitatively analyze the conformational changes during the CZD treatment, the isomer content was estimated by using a two-phase conformational model. The *trans* isomer content increased with the number of times in CZD treatment, whereas the *gauche* content decreased. The conformational changes were attributable to the extension of amorphous chains and to the morphological change of the crystallite; folded-chain crystals transformed into extended-chain crystals.

(3) The CZD-3 fibre showed a tensile modulus of 8 GPa, a tensile strength of 1.2 GPa, and a storage modulus of 8.1 GPa at 25°C. The α peak in the tan δ–temperature curve shifted to a higher temperature, and its magnitude reduced progressively with the number of times in CZD treatment. The tensile modulus was closely related to the degree of amorphous orientation factor. Although the drawing speed of the CZD treatment was faster than

that of the batchwise HT-ZD one, the CZD fibre had the mechanical properties about equal to those of the HT-ZD fibre.

ACKNOWLEDGEMENTS

We are grateful to TORAY Ltd. for the supply of nylon 66 fibres.

REFERENCES

1. Gogolewski, S. and Penneings, A. J., *Polymer*, 1985, **26**, 1394.
2. Richardson, A. and Ward, I. M., *J. Polym. Sci.*, 1981, **19**, 1549.
3. Acierno, D., La Mantia, F. P., Polizotti, G., Alfonso, G. C. and Ciferre, A., *J. Polym. Sci. Polym. Lett. Ed.*, 1977, **15**, 323.
4. Zachariades, A. E. and Poter, R. S., *J. Appl. Polym. Sci.*, 1979, **24**, 1371.
5. Kunugi, T., Akiyama, I. and Hashimoto, M., *Polymer*, 1982, **23**, 1193.
6. Suzuki, A., Maruyama, S. and Kunugi, T., *Kobunshi Ronbunsyu*, 1992, **49**, 741.
7. Suzuki, A. and Endo, A., *Polymer*, 1997, **38**, 3085.
8. Suzuki, A., Murata, H. and Kunugi, T., *Polymer*, 1998, **39**, 1351.
9. Suzuki, A., Sato, Y. and Kunugi, T., *J. Polym. Sci. Polym. Phys. Ed.*, 1998, **36**, 473.
10. Kunugi, T., Suzuki, A. and Hashimoto, M., *J. Appl. Polym. Sci.*, 1981, **26**, 1951.
11. Keller, A., in *Growth and Perfection of Crystals*, ed. D. Turnbull. John Wiley and Sons, New York, 1958.
12. Wilchainsky, Z. W., *J. Appl. Phys.*, 1959, **30**, 79.
13. Matumoto, K., *Sen-i Gakkaishi*, 1970, **32**, T–365.
14. O'Neill, M. A., Duckett, R. A. and Ward, I. M., *Polymer*, 1988, **29**, 54.
15. Peszkin, P. N. and Schultz, J. M., *J. Polym. Sci.*, 1986, **24**, 2591.
16. Murthy, N. S., Gray, R. G., Correale, S. T. and Moore, R. A. F., *Polymer*, 1995, **36**, 3863.
17. Quintanilla, L., Rodríguez-Cabello, J. C. and Pastor, J. M., *Polymer*, 1994, **35**, 2321.
18. Quintanilla, L., Rodríguez-Cabello, J. C., Jawhari, T. and Pastor, J. M., *Polymer*, 1994, **34**, 3787.
19. Elenga, R., Seguela, R. and Rietsch, F., *Polymer*, 1991, **32**, 1975.
20. Fakirov, S., Fischer, E. W., Hoffmann, R. and Schmidt, G. F., *Polymer*, 1977, **18**, 1121.
21. Wills, A. J., Capaccio, G. and Ward, I. M., *J. Polym. Sci. Polym. Phys. Ed.*, 1980, **18**, 493.
22. Gaymans, R. J., Van Utteren, T. E. C., Van Der Berg, J. W. A. and Schuyer, J., *J. Polym. Sci. Polym. Chem. Ed.*, 1977, **15**, 537.
23. Wilson, M. P. W., *Polymer*, 1974, **15**, 277.
24. Choy, C. L., Leung, W. P. and Ong, E. L., *Polymer*, 1985, **26**, 884.
25. Ghanem, M. A. and Porter, R. S., *J. Polym. Sci. Part B*, 1989, **27**, 2587.
26. Mochizuki, M. and Kudo, K., *Sen-i Gakkaishi*, 1991, **47**, P–337.
27. Gianch, J., Spruiell, J. E. and Clark, E. S., *J. Appl. Polym. Sci.*, 1982, **27**, 3527.
28. Papir, Y. S., Kapur, S., Rogers, C. E. and Baer, E., *J. Polym. Sci.*, 1972, **10**, 1305.